# Nonlinear Convex Optimization of the Energy Management for Hybrid Electric Vehicles

S. Meo, *Senior Member, IEEE*

***Abstract*—In the last years, the increase of electrical/electronic components in vehicles combined with new governmental standards to comply more stringent exhaust gas emission levels encourage for the introduction of energy control strategies that ensure optimum energy management for all the vehicle operative conditions avoiding, in the same time, a negative impact on the power train performances and on the fuel economy. The paper proposes a new energy management strategy oriented to the minimization of the fuel consumption and pollutant emissions in hybrid electric vehicles. In the paper this minimization has been formulated as a nonlinear convex optimization problem on the base of an accurate modeling of the vehicle validated on a commercial car. Although a power-split hybrid electric vehicle has been considered for the formulation of the strategy, the adopted methodology is suitable for any hybrid configuration (parallel, serie-parallel, etc). In the paper, after a full description of the proposed strategy its validity has been tested on an effective commercial vehicle proving the goodness of the proposal.**

***Index Terms*—Power-split hybrid electric vehicles, energy management, optimal control, fuel reduction, emissions reduction, automotive electric power system**

## I. Introduction

Recently, with the increase of electrical/electronic components in vehicles, the on-board electric power requirement is continuously growing for the non-propulsion loads.

The increase in power demand is due principally to the emerging automotive technologies, such as the variable engine valve, the active suspension and all the x-by-wire technologies (e.g. steering-by-wire, brake-by-wire, etc.) and the heated catalytic converter [1].

At the same time, new governmental standards force automotive manufacturers to comply with the stringent exhaust gas emission levels [2].

In order to avoid a negative impact on the power train performances and on the fuel economy, the expanding electrical system functions and the required reduction of consumptions and pollutant emissions call for the introduction of energy control strategies that ensure the electrical system robustness and the optimum energy management for all the vehicle operative conditions.

The aim of any energy management strategy for a parallel hybrid electric vehicle, as for a power-split architecture, is to split the power for the propulsion between the mechanical and electric path, in order to reduce the fuel consumption and/or the engine emissions, unaffecting the drivability of the vehicle and the on-board electrical loads supplies.

To achieve these targets, several approaches have been investigated in the last years.

These approaches can be distinguished in two classes: the first concerns the real-time control strategies that can be used to control the vehicle; the second class of algorithms deals with the application of global optimization methods on the basis of the knowledge of the drive cycle and other information about the state of the vehicle.

In the first class, several algorithms have been suggested [3]-[13], some of which use fuzzy logic controllers, model predictive controller, Equivalent Consumption Minimization Strategy (ECMS)-type control, rules based expert systems or other controllers based on an energy-flow analysis. In the second class many algorithms based on linear programming, optimal control and dynamic programming have been proposed [14]-[24].

In general the algorithms of the second class do not offer a real-time solution because they assume that the drive cycle is entirely known. In addition, they require a lot of computational time and a fine tuning of their parameters, therefore their use is restricted to single experiments and for a fixed drive cycle. Nevertheless, their results can be very interesting, because it can be used as a benchmark for the performance of other strategies, or to derive rules for the rule-based strategies.

However, many of these techniques have not been tested on commercial vehicles. Their results are relevant to the theoretical architectures of hybrid vehicles (series, parallel, parallel-series) or prototype realizations, therefore their significance is poor. To outperform these algorithms, a particular approach based on the optimal control theory is proposed in this paper and a concrete case study has been reported for a validation of the strategy.

In the paper, the problem of optimizing the fuel consumption and the pollutant emissions has been formulated as a nonlinear convex optimization problem, for a commercial power-split hybrid electric vehicle. Specifically, the Toyota Prius NHW10 model has been considered as a case study for the simulations and the related data given from the manufacturer or present in literature have been adopted.

The paper is arranged as follows: in section II, the considered vehicle and its model are presented; in section III, the control strategy is depicted; in section IV, the numerical simulations results are presented and discussed; in section V, the conclusions are resumed.

Manuscript received August 08, 2014; revised October 07, 2014.

S. Meo is with the Department of Electrical Engineeringand Information technology (DIETI), Federico II University of Naples, 21 Claudio – I80125 Naples Italy; e-mail: santolo@unina.it).

## II. Vehicle Modeling

### A. The Considered Hybrid Architecture

There are several hybrid vehicle architectures that could be considered for the application of the proposed Optimization Strategy. In the next, the Toyota® Prius NHW10 model will be considered; it is a full-hybrid vehicle with a Continuously Variable Trasmission (CVT). The proposed method can be easily extended to other hybrid architectures. The Prius NHW10 model (Fig. 1) is known as Hybrid Synergy Drive [25]. It incorporates the following items:

1. The ICE uses the more efficient Atkinson cycle instead of the more common Otto cycle; it provides 43 kW (58 hp) @ 4000 rpm and 102 Nm @ 4000 rpm;
2. An electric motor (500 V PM brushless), providing 30 kW (40 hp) @ 940 rpm and 305 Nm torque @ zero speed;
3. An electric generator (500 V PM brushless) which provides 15 kW @ 6000 rpm;
4. An IGBT inverter controlled by a 32-bit microprocessor, which efficiently converts power between the batteries and the motor/generators;
5. The regenerative braking, a process for recovering the kinetic energy when braking or traveling down a slope and storing it as the electrical energy in the traction battery for later use while reducing the wear and the tear on the brake pads;
6. The sealed 240-cell nickel metal hydride (NiMH) battery providing 300 volts, 4.3 MJ rated capacity, 25 kW max. output power;
7. The CVT — the Prius does not use a typical CVT; Toyota calls it the Power Split Device. The electric machines and gasoline engine are connected to a planetary gear set which is always engaged, and there is no shifting.

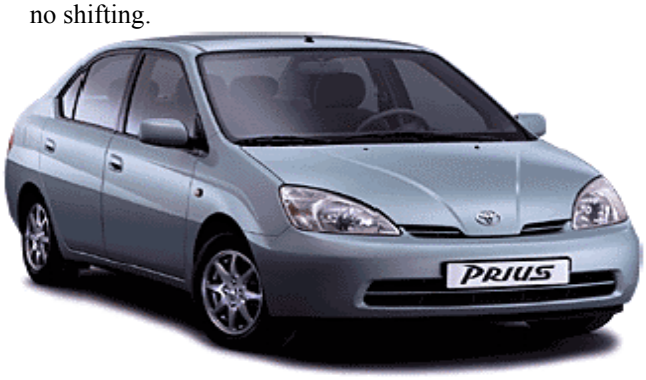


Fig. 1. The NHW10 model of TOYOTA PRIUS [25].

### B. Basic Assumptions

For the formalization of the vehicle modeling the following assumptions are made:

- The drive cycle is known;
- The sampling interval of the control strategy is sufficiently large (1 s or larger) so that to neglect the dynamic behavior of the engine, of the electric motor and of the generator: their characteristics can be represented by static models;
- The control strategy guarantees that the drivability of the vehicle remains unaffected, therefore at each time instant the drive train power, as well as the vehicle speed, are known;
- The power required from the electric loads is assigned;
- The voltage on the electrical bus is constant;
- The battery losses don't depend on the temperature.

Fig. 2 shows a power flow diagram of the vehicle.

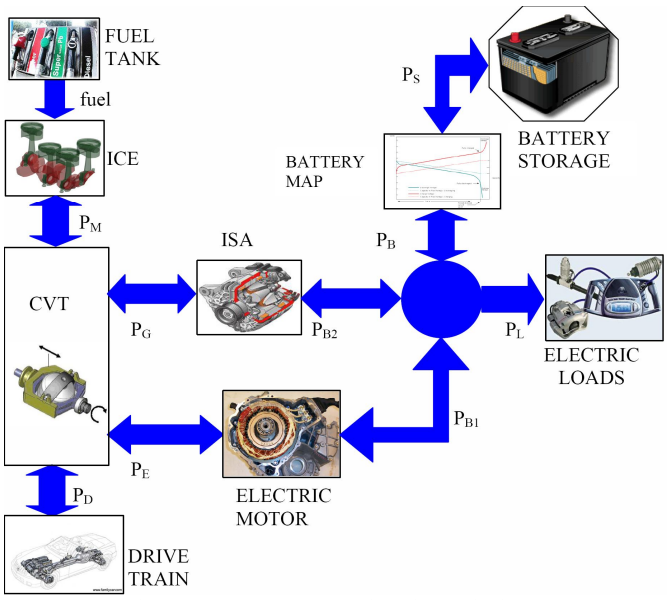


Fig. 2. Power flow diagram of a power-split hybrid vehicle.

The data used for modeling the components of the vehicle are the experimental data available on NREL web site [26].

According to the previous assumptions, the modeling of each effective component of the considered Toyota Prius (see Fig. 2) has been formulated as reported in the following.

*Engine*

Fig. 3 shows a view of the Toyota Prius ICE. It implements an Atkinson's cycle. For this component, a static model of the fuel consumptions and the pollutant emissions has been adopted.

*Consumption model*

It is assumed that the fuel rate consumption $\dot{m}_f\left(P_M, n\right)$ depends on the engine power ($P_M$) and the engine speed ($n$) by means of a nonlinear, memoryless function (static map)

Fig. 4 shows the fuel map of the 1.5L Prius engine with Atkinson cycle, as a function of the engine mechanical power, for different engine speeds.

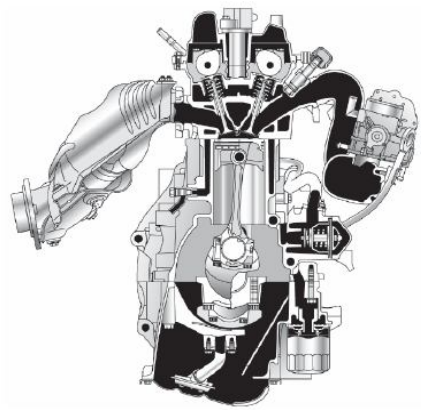

Fig. 3. The Toyota Prius internal combustion engine.

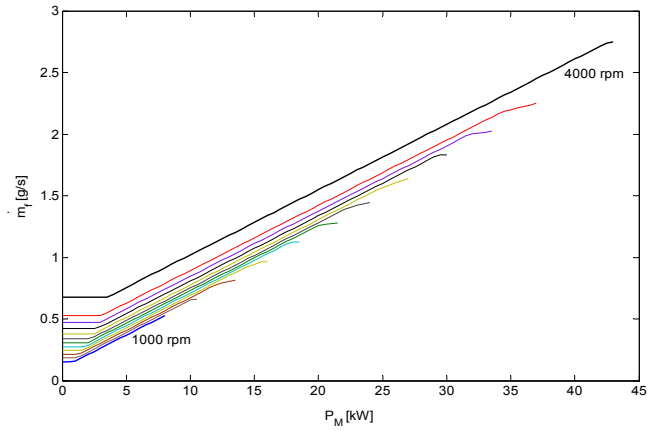


Fig. 4. Fuel map of a 1.5L Prius (Atkinson cycle) engine (by Feng An's model [26]).

*Emissions model.*

The pollutant emissions rate (HC, CO, NOx) are denoted with $\dot{m}_{HC}(P_M, n)$, $\dot{m}_{CO}(P_M, n)$ and $\dot{m}_{NOx}(P_M, n)$ and, as the fuel rate, depend on the engine power ($P_M$) and the engine speed ($n$) by means of a nonlinear, memoryless function (static map).

Figs. 5 show the emissions maps of the 1.5L Prius engine, as a function of the engine mechanical power, for different engine speeds.

*Electric Motor*

The propulsion motor of the considered Toyota Prius (NHW10 model) is a 500 V PM brushless motor, providing 30 kW at 940 rpm and 305 Nm torque at zero speed (Fig. 6).

It is hypothesized that the efficiency of the electric motor is related to the electric power ($P_{B1}$) and to the motor speed ($n_e$) by a nonlinear, memoryless function (static map):

$$\begin{cases} \eta_e = f_e(P_{B1}, n_e) \\ P_E = P_{B1}\eta_e^{sign(P_{B1})} \end{cases} \tag{1}$$

Fig. 7 shows the efficiency map of the brushless motor, as a function of the input electric power and of the motor speed [26].

Fig. 8 shows the maximum mechanical power and the torque developed by the electric motor, over the whole range of speed [26].

*Power Train*

The power $P_M$ given from the engine is splitted into a part needed for the propulsion and a part that will be converted in electric power from the generator, for the electric loads and the battery recharging.

The power $P_D$ needed for propulsion is related to the vehicle velocity $v$, acceleration $\dot{v}$ and road slope $h$ as follows:

$$P_D(t) = f_d\left[v(t), \dot{v}(t), h(t)\right] \tag{2}$$

The function $f_d$ includes the aerodynamic and rolling losses, the acceleration power and the power related to the changes of the vehicle's altitude. This relationship is typically expressed as follows:

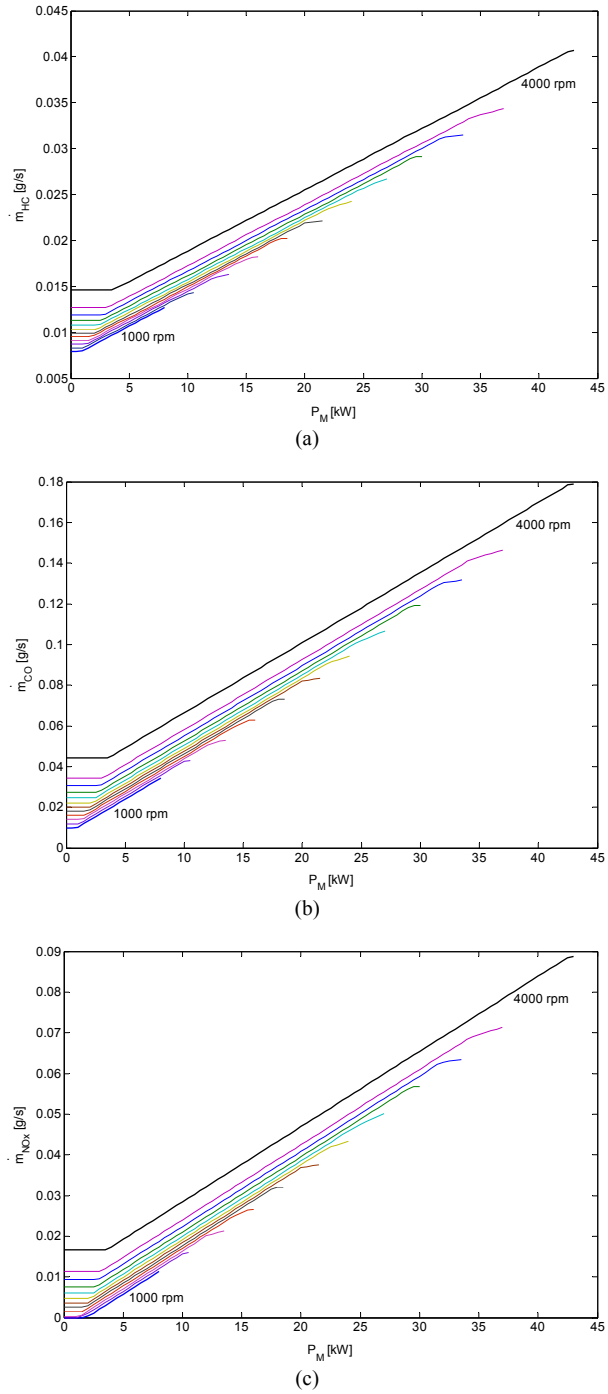


Figs. 5. Emissions maps of a 1.5L Prius (Atkinson cycle) engine: (a) HC rate map, (b) CO rate map, (c) NOx rate map (by Feng An's model [26]).

$$f_d(v, \dot{v}, h) = \left[m\dot{v} + \frac{1}{2}\rho C_d A v^2 + mg\left(C_r + \frac{h}{100}\right)\right]v \tag{3}$$

*Continuously Variable Transmission*

A fundamental component of the Prius transmission is an epicyclic gear defined "Power Split Device" (PSD).

This type of gear is also known as "sun-and-planets" because it consists of a number of "planet" gears surrounding a central "sun" gear. The planet gears are on shafts fixed to a "planet carrier", which revolves around the same axis like the sun. The planet gears are surrounded by and meshed with an inside-out gear called the "ring". Also this revolves around the same axis like everything else [25], [27], [28].

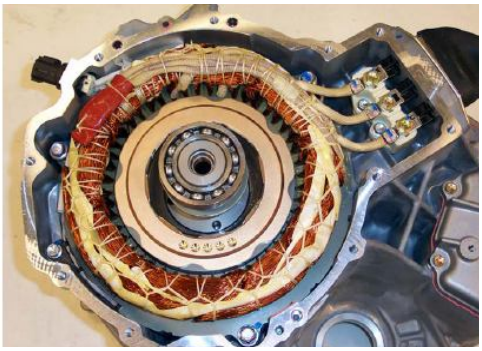

Fig. 6. The Toyota Prius electric motor.

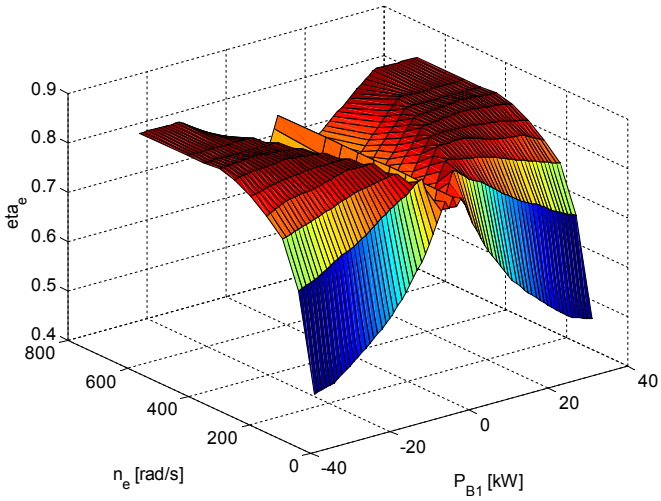


Fig. 7. The two-quadrant efficiency map of the electric motor [26].

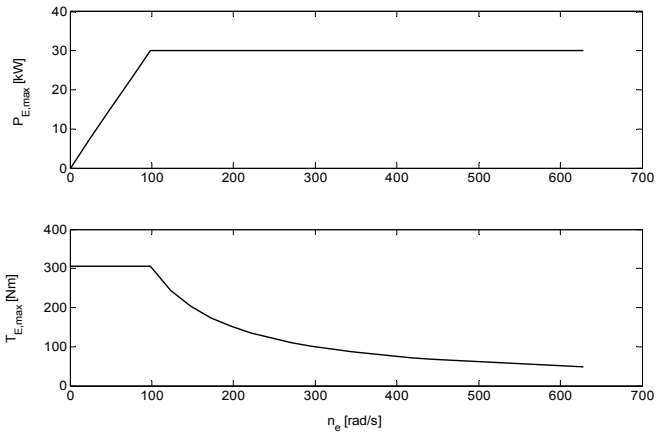


Fig. 8. Maximum mechanical power and torque of the electric motor [26].

Fig. 9 shows a schematic representation of the power split device adopted in the Toyota Prius vehicle.

The Prius internal combustion engine (ICE) is connected to the planet carrier. As it rotates, the planets mesh with and tend to push both the sun gear (in the middle) and the ring gear (around the outside) in the same direction like the planet carrier. By a careful choice of the size (and hence of the number of teeth) of the sun and the ring gears, Toyota has arranged 72% of the torque to go to the ring and 28% to go to the sun. For a given speed profile of the vehicle, the engine speed is related to the generator speed and the electric motor speed by means of the following relation:

$$n_g = n + \frac{1}{\tau}\left(n_e - n\right) \tag{4}$$

with:

$$\begin{cases} n_e = F_r n_w \\ n_w = v/R \end{cases} \tag{5}$$

Fig. 10 shows the graphic relation among the planet gears carrier (ICE), the sun gear (ISA) and the gear (drive traction) speeds, for different operative conditions of the vehicle.

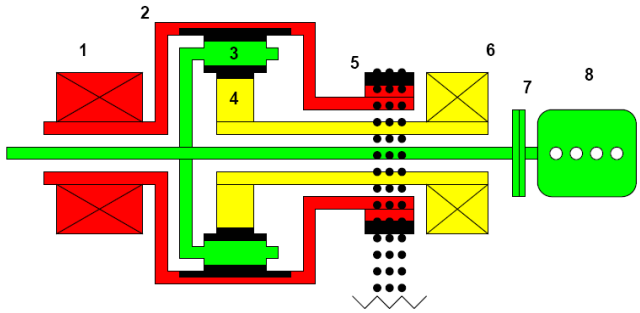


1- *electric motor*
2- ring
3- planet gears carrier
4- sun gear
5- drive traction
6- *generator*
7- vibration damper
8- *ICE*

Fig. 9. Schematic representation of the CVT in the Toyota Prius.

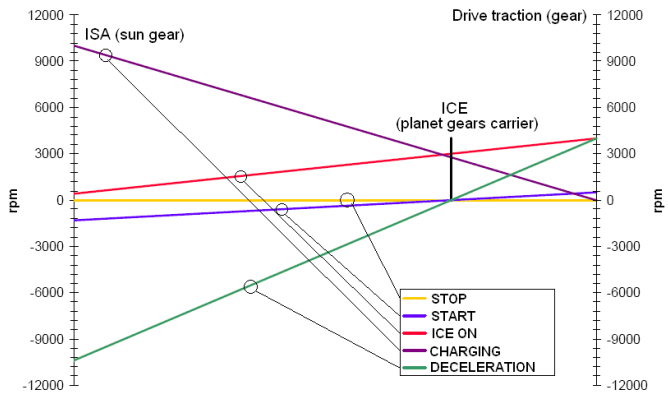


Fig. 10. Graphic relation among speeds in the CVT.

*Generator (ISA)*

The electric generator (ISA) of the considered Toyota Prius (NHW10 model) is a 500 V PM brushless which provides 15 kW at 6000 rpm. Because of the adopted sampling time, also the generator modeling is reduced to a static nonlinear map. This map relates the mechanical power $P_G$ in input to the generator with the electric power $P_{B2}$ in output from the generator. It gives the efficiency of the generator for all the operative conditions:

$$\eta_g = f_g\left(P_{B2}, n_g\right) \tag{6}$$

$$P_G = \frac{P_{B2}}{\eta_g} \tag{7}$$

Fig. 11 shows the efficiency map of the brushless generator, as a function of electric power and of the

generator speed [26]. Fig. 12 shows the maximum electric power and the maximum torque developed by the generator, over the whole range of speed [26].

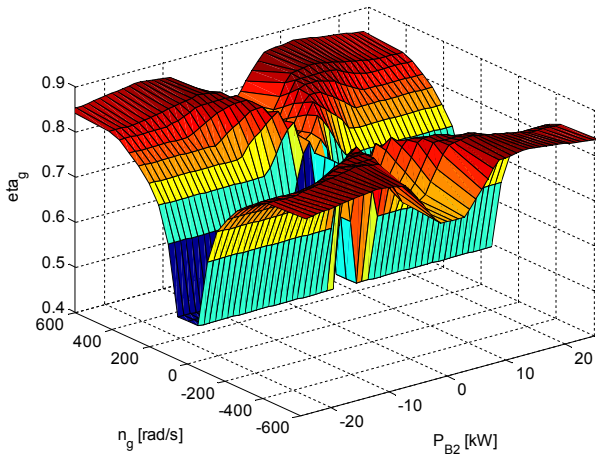


Fig. 11. The four-quadrant efficiency map of the generator [26].

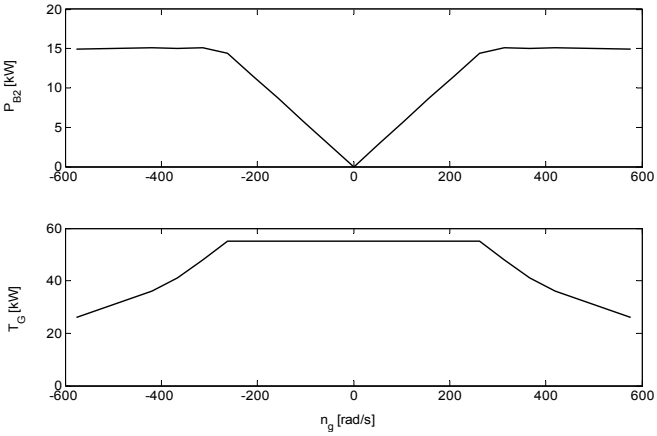


Fig. 12. Maximum electric power and torque of the generator [26].

Like a relationship between $P_G$ and $P_{B2}$, hereafter it will be adopted the maximum efficiency curve in the operative region delimited by the maximum electric power curve (Fig. 12):

$$P_{B2} = f_{g,\eta_{g\,max}}\left(n_g\right) \tag{8}$$

*Battery*

The Toyota Prius battery is a sealed 240-cell nickel metal hydride (NiMH) battery providing 300 volts, 4.3 MJ capacity. In the following, the battery has been considered as a voltage source $U_b$ controlled by the output current $i_b$ and its state of charge $Q$ (SOC), with one resistance in series $R_b$.

In particular, the voltage $U_b$ and the resistance $R_b$ in the following are given by polynomial expressions of the current and state of charge [29]:

$$U_b = \sum_{k=1}^{4} Q^{k-1} \sum_{h=1}^{2} a_{hk}\, i_b^{h-1} \tag{9}$$

$$R_b = \sum_{h=1}^{2} b_h Q^h \tag{10}$$

$a_{ij}$ are the coefficients of two 2×4 matrixes, one for the charge and one for the discharge operations; these depend on the kind of batteries used.

The power $P_B$ in input or in output from the battery is the algebraic addition of the power $P_S$ (positive in the charging mode, negative in the discharging mode) actually stored in the battery and the battery losses that are supposed like a polynomial (quadratic) function of $P_S$, and they are positive for both the charging and discharging conditions:

$$P_B = P_S + P_{B,loss} \tag{11}$$

$$P_{B,loss} = \beta P_S^2 \tag{12}$$

with:

$$\beta = \frac{R_b}{U_b^2} \tag{13}$$

The battery energy level $E_s$ is given by:

$$E_S(t) = E_S(0) + \int_0^t P_S(\tau)\, d\tau \tag{14}$$

The state of charge is defined as:

$$Q(t) = \frac{E_s(t)}{C_b} \tag{15}$$

The model is completely assigned if $R_b$ in charging and discharging mode (Figs. 13, 14) and $U_b$ (Fig. 15) are assigned over all the SOC range [26].

*On-board Electrical Loads*

The electric power profile adopted for the modelling of the on-board electrical loads has been computed with the *Critical Loads Activation Sequences Maker* tool, that is part of ***EVALUATOR®*** suite, developed by the same Author [30].

Such technique generates, by means of a stochastic approach, different sequences of loads activation and it gives, as output, a set of critical operative conditions suitable for testing the power source system.

In Fig. 16, a schematic of the electrical power bus of a hybrid electric vehicle is represented, with some of the electrical loads actually available on modern hybrid/conventional vehicles, such as: throttle-by-wire, power steering, anti-lock braking, rear-wheel steering, air-conditioning, ride-height adjustment, active suspension, electrically heated catalyst, and so on [1].

## III. The Proposed Control Strategy

The aim of the proposed control strategy is to split the power for the propulsion between the thermal and electric path, in order to minimize the fuel consumption and the engine emissions, unaffecting the drivability of the vehicle and the on-board electrical loads requests.

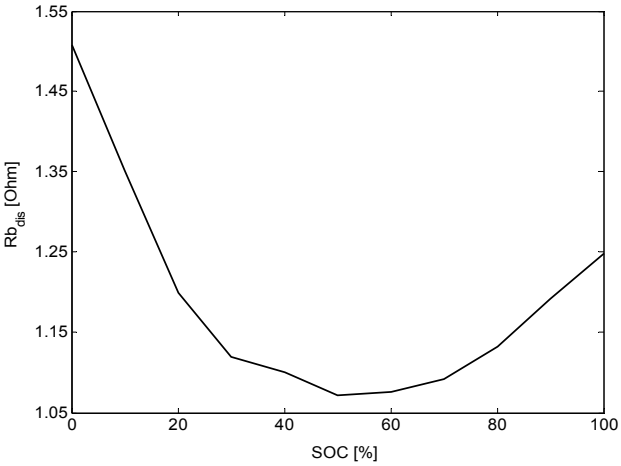


Fig. 13. Toyota Prius battery equivalent resistance in discharging mode [26].

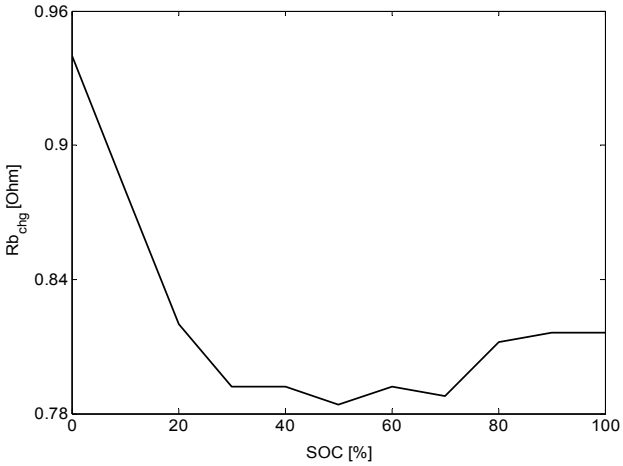


Fig. 14. Toyota Prius battery equivalent resistance in charging mode [26].

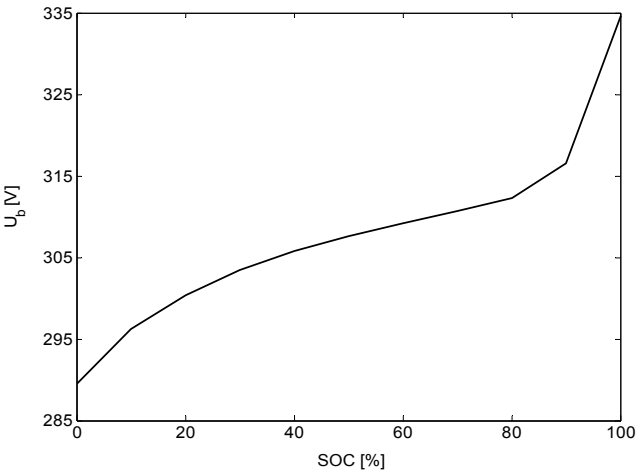


Fig. 15. Toyota Prius battery open-circuit voltage [26].

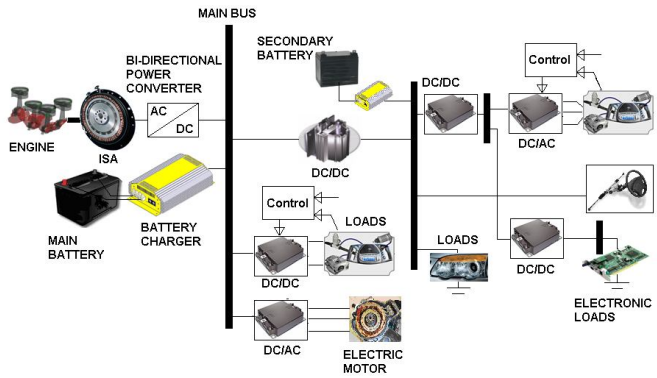


Fig. 16. Vehicle electrical power system architecture.

This target can be achieved shifting the engine operating point versus regions with the maximum efficiency, realizing an optimal power split between engine and electric motor.

Nevertheless, in order to unaffecting the drivability of the vehicle, both the ISA generator output power $P_{B2}$ and the electric motor output power $P_E$ must be adequately controlled. In fact, the electric motor and the generator are coupled to the engine by means of CVT (Fig. 2) therefore, controlling their generated powers, the operating power and speed of the combustion engine will be influenced.

The battery can be recharged even by means of re-generative braking; this is possible by controlling the electric motor as a generator during the braking mode.

The action of the proposed strategy implicates that the battery is not used, like in a conventional vehicle, only to supply key-off loads and to assist the alternator against peak-power demands, but it is also used to satisfy the request of the electric motor for propulsion.

The power $P_B$ flows in output or in input from the battery depending on the necessity of the control strategy to shift the engine operating point versus regions with maximum efficiency.

Let us consider $T_s$ the sampling time of the control strategy, indicating with $k$ the *k-mo* sampling period and considering the equations (1), (4), (6)-(7), (11)-(12), the energetic model of the vehicle, in discrete time, is given by the following system of equations (the generic quantity $f(k) \equiv f(kT_s)$ ):

$$\begin{cases} P_{B2}(k) = P_B(k) + P_L(k) + P_{B1}(k) \quad \text{(electrical node)} \\ \left.\begin{array}{l} P_M(k) + P_E(k) = P_G(k) + P_D(k) \\ n_g(k) = n(k) + \dfrac{1}{\tau}\left[F_r n_w(k) - n(k)\right] \end{array}\right\} \text{(mechanical node)} \\ P_{B2}(k) = f_{g,\eta_{g\,max}}\left(n_g(k)\right) \\ P_G(k) = \dfrac{P_{B2}(k)}{f_g\left(P_{B2}(k), n_g(k)\right)} \\ P_E(k) = P_{B1}(k)\left[f_e\left(P_{B1}(k), n_e(k)\right)\right]^{sign\left(P_{B1}(k)\right)} \\ P_B(k) = P_S(k) + \beta P_S^2(k) \end{cases} \tag{16}$$

with the following conventional signs:

- $P_G > 0$ if in output from the mechanical node;
- $P_D > 0$ if in output from the mechanical node;
- $P_M > 0$ if in output from the engine;
- $P_B > 0$ if in output from the electrical node;
- $P_{B1} > 0$ if in output from the electrical node;
- $P_{B2} > 0$ if in output from the generator;
- $P_E > 0$ if in output from the electric motor.

At the istant $k$, the system (16) is a system of 6 equations in 8 unknown quantities. It can be resolved respect to two quantities.

In the following, all the quantities will be expressed respect to the battery storage power $P_S$ and the engine speed $n$. This consents to write also the power $P_M$ as function of $P_S$ and $n$:

$$P_M(k) = f_M\left(n(k), P_S(k), P_S(k-1), \ldots, P_S(1)\right) \tag{17}$$

Indicating with $T_c$ the period of the considered drive cycle, the total fuel used at the end of the cycle is given by:

$$F = \int_0^{T_c} f_{tot}(t)\,dt \tag{18}$$

with:

$$\begin{aligned} f_{tot} &= k_1 \dot{m}_f(P_M, n) + k_2 \dot{m}_{HC}(P_M, n) + \\ &\quad k_3 \dot{m}_{CO}(P_M, n) + k_4 \dot{m}_{NOx}(P_M, n) \end{aligned} \tag{19}$$

where $k_1$, $k_2$, $k_3$, $k_4$ are defined constants [20].

The goal of the control strategy is to minimize the cost function (18) [31].

Because the ranges of the different quantities involved in the power diagram (Fig. 2) are limited by physics underlying or by engineering design, the control strategy can be formulated as a nonlinear optimization problem subject to constraints. In particular, the following inequality constraints must be imposed:

$$\begin{aligned} n_{min} &\le n \le n_{max} \\ n_{gmin} &\le n_g \le n_{g\,max} \\ P_{M\,min} &\le P_M \le P_{M\,max} \\ P_{E\,min} &\le P_E \le P_{E\,max} \\ P_{S\,min} &\le P_S \le P_{S\,max} \end{aligned} \tag{20}$$

The battery is constrained to have the same amount of energy at the start of the drive cycle and at the end:

$$E_s(T_c) = E_s(0) \tag{21}$$

By considering the basic assumptions and the equation (17), in discrete time the relation (19) can be expressed as a function of the battery storage power and the engine speed only, as follows:

$$\begin{aligned} &f_{tot}\left(P_M(k), n(k)\right) = \\ &\quad f'_{tot}\left(n(k), P_S(k), P_S(k-1), \ldots, P_S(1)\right) \end{aligned} \tag{22}$$

Considering equation (4), the following kinematics constraints:

$$\begin{aligned} n_{min}(k) &\le n(k) \le n_{max}(k) \\ n_{g\,min}(k) &\le n_g(k) \le n_{g\,max}(k) \end{aligned} \tag{23}$$

can be translated to constraint on $n$ only:

$$n'_{min}(k) \le n(k) \le n'_{max}(k) \tag{24}$$

with:

$$\begin{aligned} n'_{min}(k) &= max\left\{ n_{min}(k), \frac{n_{g\,min}(k) - \frac{n_e(k)}{\tau}}{1 - \frac{1}{\tau}} \right\} \\ n'_{max}(k) &= min\left\{ n_{max}(k), \frac{n_{g\,max}(k) - \frac{n_e(k)}{\tau}}{1 - \frac{1}{\tau}} \right\} \end{aligned} \tag{25}$$

Referring to the system of equations (16), the following dynamics constraints:

$$\begin{aligned} 0 &\le P_M(k) \le P_{M\,max}\left(n(k)\right) \\ -P_{E\,max}\left(n_e(k)\right) &\le P_E(k) \le P_{E\,max}\left(n_e(k)\right) \\ P_{S\,min}(k) &\le P_S(k) \le P_{S\,max}(k) \end{aligned} \tag{26}$$

can be translated to constraint on $P_M$ and $P_S$ only:

$$\begin{aligned} P'_{M\,min}(k) &\le P_M(k) \le P'_{M\,max}(k) \\ P_{S\,min}(k) &\le P_S(k) \le P_{S\,max}(k) \end{aligned} \tag{27}$$

with (eq. (28)):

$$\begin{aligned} &P'_{M\,min}(k) = \\ &max\left\{0, P_D(k) + P_G(k) - P_{E\,max}\left(n_e(k)\right)\right\} \\ &P'_{M\,max}(k) = \\ &min\left\{P_{M\,max}\left(n(k)\right), P_D(k) + P_G(k) + P_{E\,max}\left(n_e(k)\right)\right\} \end{aligned} \tag{28}$$

In this way, the optimization problem statement is expressed with the following equations (N is integer and it is the ratio between the length of the drive cycle $T_c$ and the sampling time $T_s$):

$$\min_{\begin{bmatrix} n(1),\ldots,n(N) \\ P_s(1),\ldots,P_s(N) \end{bmatrix}} F = min\left\{ T_s \sum_{k=1}^{N} f'_{tot}\left(P_s(k), n(k)\right) \right\} \tag{29}$$

subject to (24), (27) and to the following equality constraint:

$$\sum_{k=1}^{N} P_S(k) = 0 \tag{30}$$

The problem is now formulated as a finite dimensional nonlinear optimization problem. Because all functions involved in the problem are convex functions, the formulated problem is a nonlinear convex problem with inequality and equality constraints [32]. The solution of this problem is given from the Kuhn-Tucker (KT) conditions [32]: for a nonlinear convex problem, KT equations are both necessary and sufficient for a global solution point.

Let us consider the problem (28) of minimizing the function $F(\mathbf{x})$ subject to $m$ equality constraints $G_i(\mathbf{x})=0$ ($i \in [1, m]$), and $p$ inequality constraints $H_j(\mathbf{x}) \le 0$ ($j \in [1, p]$).

If $\mathbf{x}_0$ is a local minimum for the constrained problem and

if it is a regular point, the KT conditions ensure that there is a vector $\boldsymbol{\lambda} = \left[\lambda_i, \lambda_j\right]_{\substack{i\in[1,m] \\ j\in[1,p]}}$ with *(m+p)* components, such that:

$$\begin{cases} \nabla_x L(\mathbf{x}_0, \boldsymbol{\lambda}) = 0 \\ \lambda_i G_i(\mathbf{x}) = 0 \quad \text{for } i \in [1,m] \\ \lambda_j H_j(\mathbf{x}) = 0 \quad \text{for } j \in [1,p] \\ G_i(\mathbf{x}) = 0 \quad \text{for } i \in [1,m] \\ H_j(\mathbf{x}) = 0 \quad \text{for } j \in [1,p] \\ \lambda_j \geq 0 \quad \text{for } j \in [1,p] \end{cases} \tag{31}$$

where:

$$L(\mathbf{x}, \boldsymbol{\lambda}) = F(\mathbf{x}) + \sum_{i=1}^{m} \lambda_i G_i(\mathbf{x}) + \sum_{j=1}^{p} \lambda_j H_j(\mathbf{x}) \tag{32}$$

is the Lagrange function and $\nabla$ is the linear operator nabla.

Eqs. (31) are also sufficient if the problem is convex. In our case we have (33):

$$\mathbf{x} = \left[n(1),..,n(k),..,n(N), P_S(1),..,P_S(k),..,P_S(N)\right]_{(1x2N)}$$

and (34):

$$G_i(\mathbf{x}) = \sum_{k=1}^{N} P_S(k) \quad \text{for } i = 1$$

$$H_j(\mathbf{x}) = \begin{cases} n(j) - n'_{max}(j) & \text{for } j \in [1,N] \\ -n(j) + n'_{min}(j) & \text{for } j \in [N+1,2N] \\ P_M(j) - P'_{M\,max}(j) & \text{for } j \in [2N+1,3N] \\ -P_M(j) + P'_{M\,min}(j) & \text{for } j \in [3N+1,4N] \\ P_S(j) - P_{S\,max}(j) & \text{for } j \in [4N+1,5N] \\ -P_S(j) + P_{S\,min}(j) & \text{for } j \in [5N+1,6N] \end{cases} \tag{34}$$

Here $\boldsymbol{\lambda}$ is a vector of 1x(1+6N) components, $m$=1, $p$=6N.

Now the problem (29) with constraints (24), (27), (30) reduces to solve numerically the system of equations (31), with $\mathbf{x}$, $G_i(\mathbf{x})$, $H_j(\mathbf{x})$ defined by (33), (34). The solution of the KT equations forms the basis for many nonlinear programming algorithms [33].

These algorithms attempt to compute the Lagrange multipliers directly. These methods are commonly referred as Sequential Quadratic Programming (SQP) methods, since a QP subproblem is solved at each major iteration. In particular in the paper the Schittkowski method has been adopted [34]. The method allows to closely mimic Newton's method for constrained optimization just as it is done for unconstrained optimization.

At each major iteration, an approximation is made of the Hessian of the Lagrangian function using a quasi-Newton updating method. This is then used to generate a QP subproblem whose solution is used to form a search direction for a line search procedure [35].

## IV. Numerical Results

In order to test the suggested control strategy, two sets of simulations have been developed: the first one refers to the application of the proposed strategy when a zero variation of SOC is imposed over the all drive cycle. The second one refers to a comparison between the proposed strategy and the management strategy actually implemented in Toyota Prius, as it is simulated by means of the ADVISOR® tool.

The parameters of the considered system are reported in Table I. The adopted European drive cycle [2] is reported in Fig. 17. Fig. 18 shows the electrical loads power profile. This profile has been computed with ***EVALUATOR***®, a computer-aided suite developed from the Authors [30]. All-electric compressor for cooling is not included in the considered loads, as it has been introduced in the 2004 model only.

TABLE I
Simulation Parameters

| *Symbol* | *Quantity* | *Value* | *Unit* |
|---|---|---|---|
| **SIMULATION TIME:** | | | |
| $T_c$ | Drive cycle lenght | 1180 | s |
| $T_s$ | Sample time | 1 | s |
| **VEHICLE:** | | | |
| $m$ | Mass (full load) | 1700 | kg |
| $A$ | Frontal area | 1.746 | $m^2$ |
| $C_d$ | Air drag coefficient | 0.3 | |
| $C_r$ | Rolling resistance coeff. | 0.009 | |
| $\rho$ | Air density | 1.2 | $kg/m^3$ |
| $g$ | Gravity | 9.81 | $m/s^2$ |
| $R$ | Wheel radius | 0.287 | m |
| $F_r$ | Final drive ratio | 3.93 | |
| $\tau$ | CVT ratio | -30/78 | |
| **BATTERY:** | | | |
| $U_b$ | Voltage | 300 | V |
| $C_b$ | Capacity | 6 | Ah/cell |
| | | 4354560 | J |
| $S.O.C._0$ | Initial S.O.C. | 70% | |
| $P_{Smax}$ | Maximum charging power | 25 | kW |
| **ICE:** | | | |
| $P_{Mn}$ | Nominal power | 43 | kW |
| $n_n$ | Nominal speed | 4000 | rpm |
| $T_{Mn}$ | Nominal torque | 101.7 | Nm |
| **ELECTRIC MOTOR:** | | | |
| $P_{En}$ | Nominal power | 30 | kW |
| $n_{En}$ | Nominal speed | 1000 | rpm |
| $T_{En}$ | Nominal torque | 300 | Nm |
| $V_{En}$ | Nominal voltage | 500 | V |
| **GENERATOR:** | | | |
| $P_{B2n}$ | Nominal power | 15 | kW |
| $n_{gn}$ | Maximum speed | 6000 | rpm |
| $V_{gn}$ | Nominal voltage | 500 | V |

The considered static maps for ICE, generator and electric motor are reported in Figs. 4, 5, 7, 11. Fig. 19 shows the drive train power, which is derived by the vehicle speed profile and the vehicle parameters (Table I).

### *A. Results of the Proposed Strategy Implementation*

There are several hybrid vehicle architectures that could be considered for the application of the proposed Optimization Strategy. In the following are reported the profile of the main quantities of the vehicle obtained from the power split control resulting by the proposed strategy.

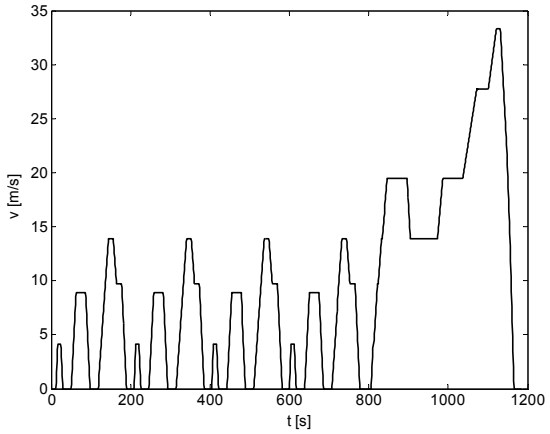


Fig. 17. New European drive cycle.

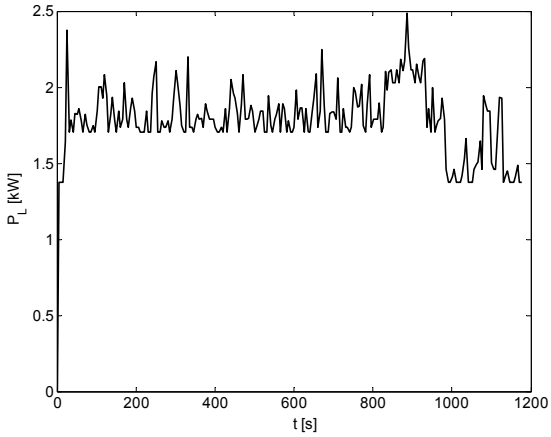


Fig. 18. Critical electrical loads power profile used for the simulation.

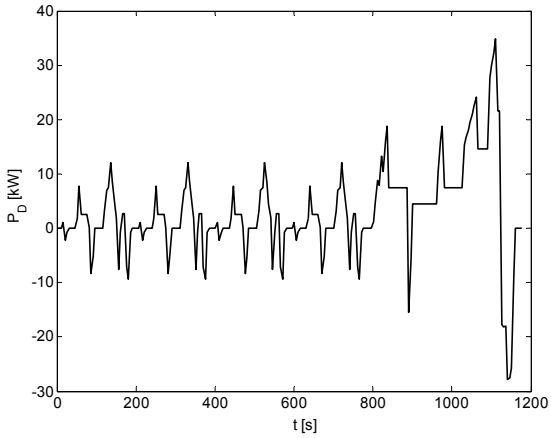


Fig. 19. Drive train power.

Figs. 20-28 show respectively the ICE speed, the ICE power, the electric motor mechanical power, the generator speed, the battery storage power (with relative bounds), the generator power, the fuel rate, the emissions rates and the battery SOC resulting by the proposed strategy. Fig. 29 shows the operative points of the ICE during the NEDC drive cycle, resulting by the proposed strategy, reported on the fuel map.

### *B. Comparisons with ADVISOR Simulations Results*

ADVISOR (Ver. 2004) is a computational tool many used for automotive applications. With ADVISOR it is possible to simulate several commercial vehicles, particularly it is possible to simulate the Toyota Prius NHW10 model, for a desired drive cycle with an imposed electrical loads power profile.

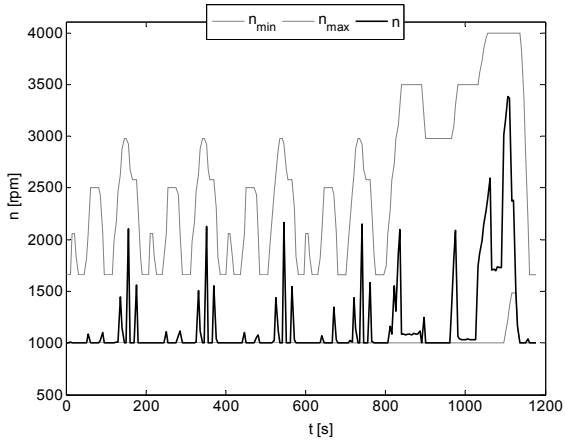


Fig. 20. Optimal ICE speed and bounds.

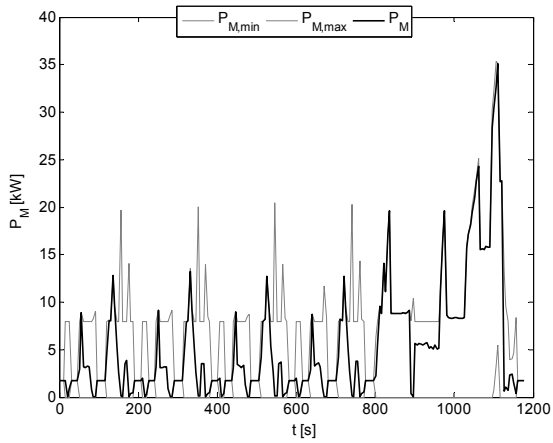


Fig. 21. Optimal ICE power and bounds.

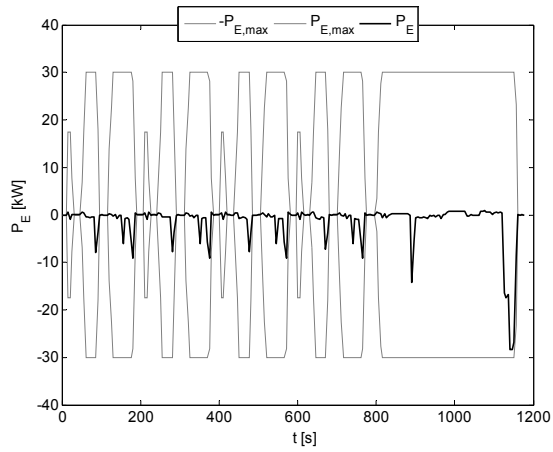


Fig. 22. Optimal electric motor mechanical power and bounds.

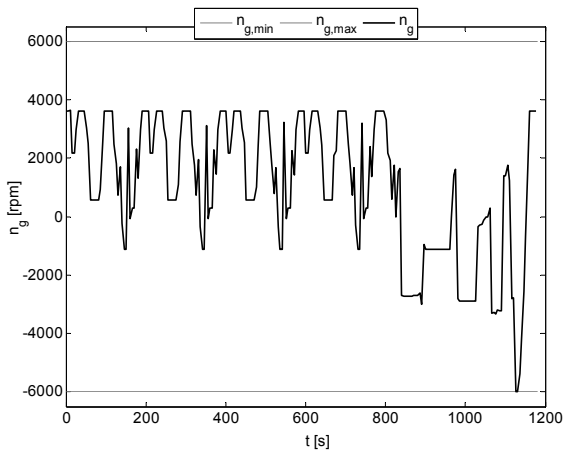


Fig. 23. Optimal generator speed and bounds.

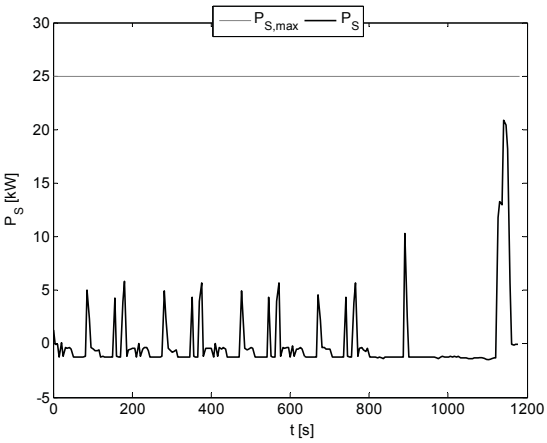


Fig. 24. Optimal battery storage power and bounds.

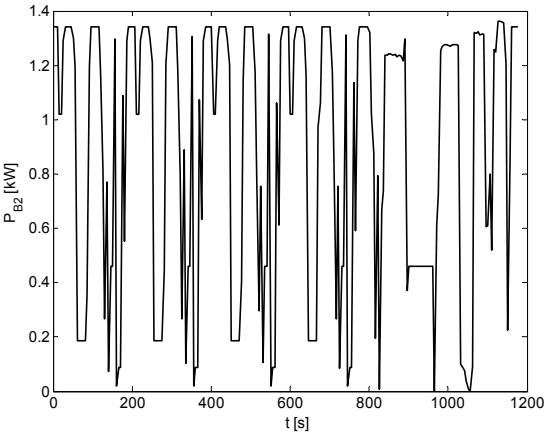


Fig. 25. Optimal generator electric power.

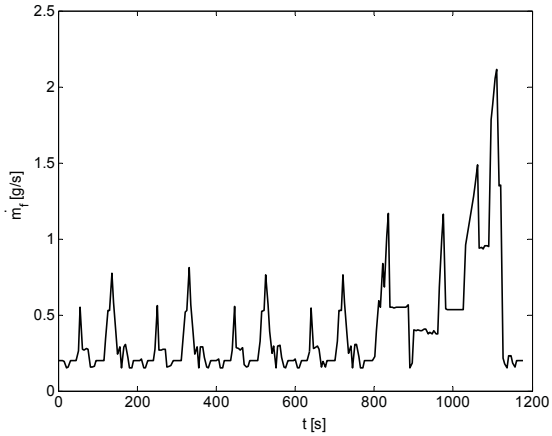


Fig. 26. Optimal fuel consumption rate.

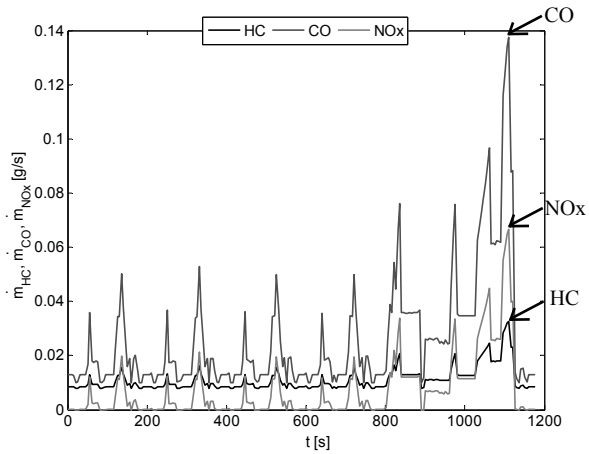


Fig. 27. Optimal emissions rate.

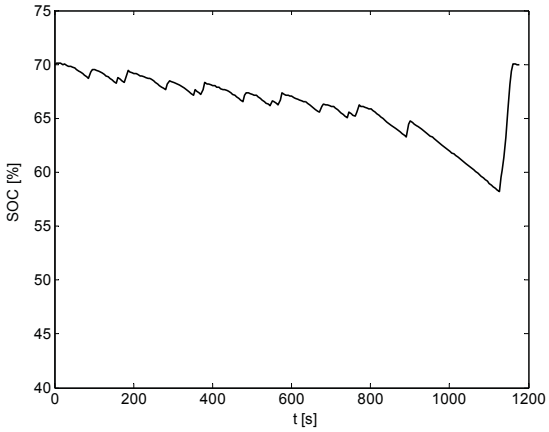


Fig. 28. Optimal battery SOC.

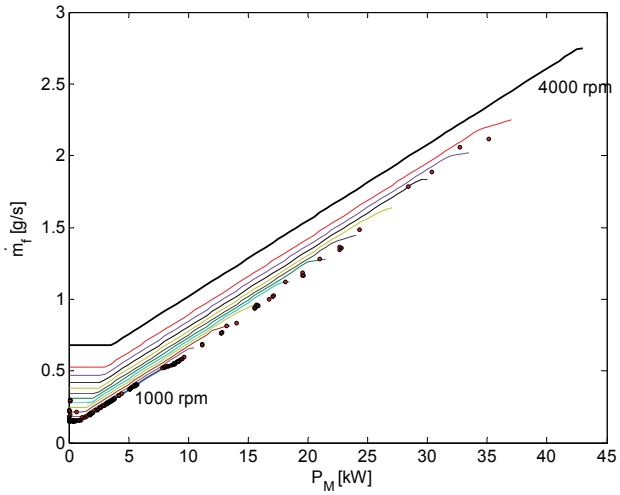


Fig. 29. Optimal operative points of ICE.

In the ADVISOR's model of Prius, the realistic Hybrid Powertrain Control Strategy is implemented; it realizes several operative modes, depending on the state of the vehicle [25].

The numerical results of ADVISOR simulations, carried out under the same operative conditions adopted for our strategy, show that the SOC at the end of the drive cycle is lower than the initial SOC, instead of the results of the proposed strategy.

Therefore, for a correct comparison between ADVISOR and the proposed strategy results, it is necessary to impose as equality constraint for the proposed strategy the following:

$$\Delta SOC_{OS} = \Delta SOC_{ADVISOR} \tag{35}$$

The constraint (30) changes consequently as follows:

$$T_s \sum_{k=1}^{N} P_S(k) = C_b \Delta SOC_{ADVISOR} \tag{36}$$

Figs. 30-35 show respectively the comparisons between ADVISOR and our strategy.

As it can be noted from Fig. 34, the philosophy of the battery's service is quite different for the two strategies. In fact, such figure shows as the two controls often impose different sign for the battery storage power.

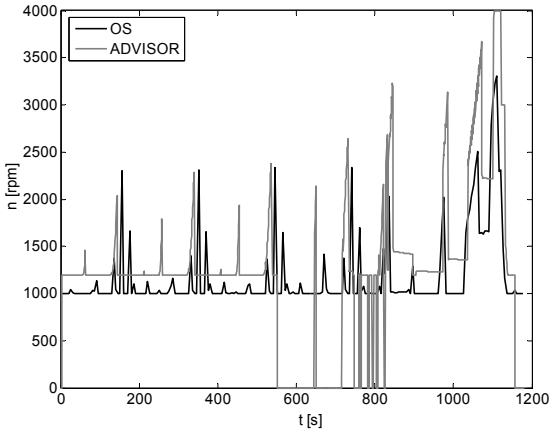


Fig. 30. Optimal vs. ADVISOR ICE speed.

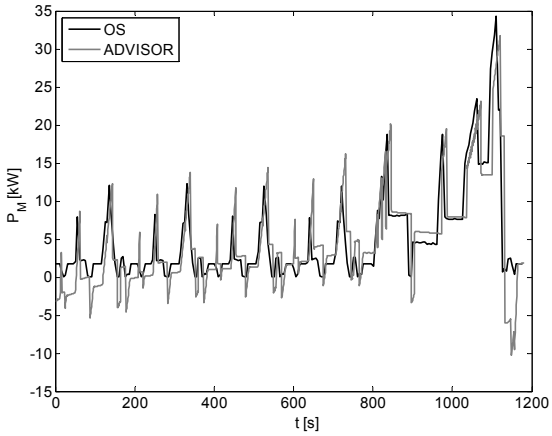


Fig. 31. Optimal vs. ADVISOR ICE power.

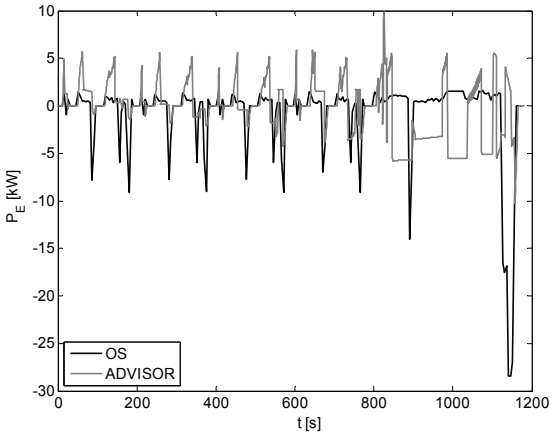


Fig. 32. Optimal vs. ADVISOR electric motor mechanical power.

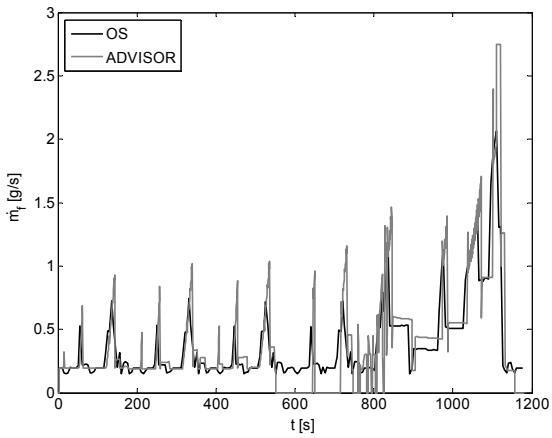


Fig. 33. Optimal vs. ADVISOR fuel consumption rate

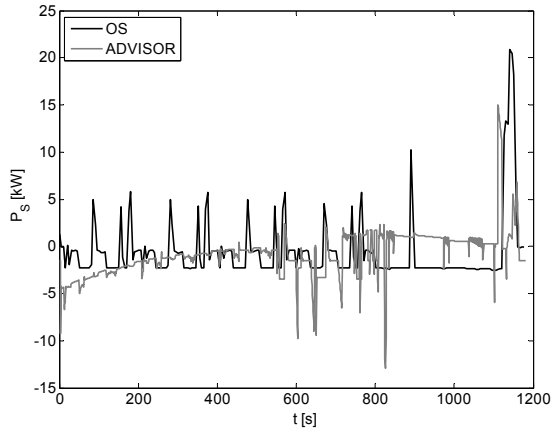


Fig. 34. Optimal vs. ADVISOR battery storage power.

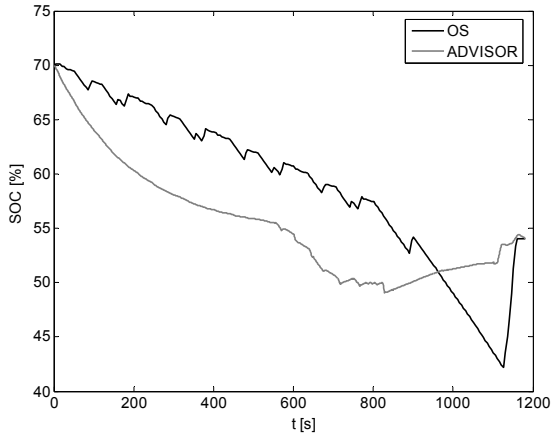


Fig. 35. Optimal vs. ADVISOR battery SOC.

As it can be noted from Fig. 35, the variation of the SOC between the start and the end of the cycle is the same for both the strategies, according to the constraint (36).

Table II presents the results comparison relative to the consumptions and the emissions.

TABLE II
COMPARISON RESULTS

| | PROPOSED STRATEGY | ADVISOR | % SAVING |
|---|---|---|---|
| FUEL [g] | 442.3 | 458.6 | 3.6% |
| HC [g] | 12.7 | 15.9 | 20% |
| CO [g] | 28.8 | 33.1 | 13% |
| NOx [g] | 7.5 | 9.5 | 21% |

The results show that with the proposed strategy a 3.6% reduction in fuel use and 20%, 13%, 21% reduction in engine emissions (HC, CO, NOx) can be obtained respect to the real consumptions and emissions of Toyota Prius, as computed by the ADVISOR.

## V. CONCLUSION

In the paper, the problem of optimizing the fuel consumption and the pollutant emissions in a power-split commercial vehicle has been formulated as a nonlinear convex optimization problem. The results show that with the proposed strategy a reduction of 3.6% in the fuel use and much more in the emissions can be obtained respect to the real consumptions and emissions of Toyota Prius, as computed by the ADVISOR. This proves the feasibility to

adopt the suggested strategy as a benchmark for the performance of other strategies, or to derive rules for rule-based strategies.

## NOMENCLATURE

| | |
|---|---|
| $m$ [kg] | Vehicle mass |
| $A$ [m$^2$] | Vehicle frontal area |
| $C_d$ | Air drag coefficient |
| $C_r$ | Rolling resistance |
| $\rho$ [kg/m$^3$] | Air density |
| $g$ [m/s$^2$] | Gravity |
| $h$ | Road slope |
| $R$ [m] | Vehicle wheel radius |
| $F_r$ | Final drive ratio |
| $G_r$ | Gear ratio |
| $-\tau$ | Sun gear teeths/ring gear teeths CVT ratio |
| $U_b$ [V] | Open-circuit battery voltage |
| $R_b$ [Ω] | Battery equivalent circuit resistance |
| $C_b$ [J] | Battery rated capacity |
| $E_s$ [J] | Battery energy level |
| $S.O.C.$ | Battery State of Charge |
| $v$ [m/s] | Vehicle linear speed |
| $n$ [rpm] | Angular speed of engine |
| $n_e$ [rpm] | Angular speed of electric motor |
| $n_g$ [rpm] | Angular speed of generator |
| $n_w$ [rpm] | Vehicle-wheels angular speed |
| $P_M$ [kW] | Internal Combustion Engine (ICE) mechanical power (without losses) |
| $P_D$ [kW] | Required propulsion power |
| $P_L$ [kW] | Required on-board electrical loads power |
| $P_G$ [kW] | Mechanical power of the generator |
| $P_{B2}$ [kW] | Electrical power of the generator |
| $P_E$ [kW] | Mechanical power of the electric motor |
| $P_{B1}$ [kW] | Electrical power of the electric motor |
| $P_B$ [kW] | Battery power (with losses) |
| $P_S$ [kW] | Battery storage power (without losses) |
| $P_{B,loss}$ [kW] | Battery losses |
| $\eta_e$ | Electric motor efficiency |
| $\eta_g$ | Generator efficiency |
| $\dot{m}_f$ [g/s] | Fuel consumption rate |
| $\dot{m}_{HC}$ [g/s] | HC emission rate |
| $\dot{m}_{CO}$ [g/s] | CO emission rate |
| $\dot{m}_{NOx}$ [g/s] | NOx emission rate |
| $F$ | Cost function |
| $k_1$, $k_2$, $k_3$, $k_4$ | Weighting factors |
| $T_c$ [s] | Period of the drive cycle |
| $T_s$ [s] | Sample period |
| $sign(x)$ | Signum function |

## REFERENCES


[1] A. Emadi, M. Ehsani, J. M. Miller, *Vehicular Electric Power Systems*, Marcel Dekker, Inc., 2004

[2] NEDC, European Council Directive, 70/220/EEC with amendments.

[3] Liu Shaohua ; Du Changqing ; Yan Fuwu ; Wang Jun ; Li Zheng ; Luo Yuan, A Rule-Based Energy Management Strategy for a New BSG Hybrid Electric Vehicle, *Intelligent Systems (GCIS), 2012 Third Global Congress on*, Page(s): 209-212

[4] Naderi, P., Samimi, A., Fuel-cell/battery hybrid vehicle modeling and fuzzy controller design for power management, (2012) *International Review on Modelling and Simulations (IREMOS)*, 5 (2), pp. 982-990.

[5] Shams-Zahraei, M., Kouzani, A.Z., Ganji, B., Effect of noise factors in energy management of series plug-in hybrid electric vehicles, (2011) *International Review of Electrical Engineering (IREE)*, 6 (4), pp. 1715-1726.

[6] Borhan, H.A. ; Vahidi, A. ; Phillips, A.M. ; Kuang, M.L. ; Kolmanovsky, I.V., Predictive energy management of a power-split hybrid electric vehicle, American Control Conference, 2009. ACC '09., Page(s): 3970 - 3976.

[7] Pisu, P. ; Rizzoni, G.,A Comparative Study Of Supervisory Control Strategies for Hybrid Electric Vehicles, Control Systems Technology, IEEE Transactions on, Volume 15 , Issue 3, 2007, Page(s): 506 - 518

[8] M. Mohebbi, M. Charkhgard, M. Farrokhi, Optimal neuro-fuzzy control of parallel hybrid electric vehicles, *Vehicle Power and Propulsion, 2005 IEEE Conference, 7-9 Sept. 2005 Page(s):26 – 30.*

[9] R. Langari, W. Jong-Seob, Intelligent energy management agent for a parallel hybrid vehicle-part II: Torque Distribution, Charge Sustenance Strategies, and Performance Results, *Vehicular Technology, IEEE Transactions on, Vol. 54, Issue 3, May 2005 Page(s):935 – 953.*

[10] V. H. Johnson, K. B. Wipke, D. J. Rausen, HEV control strategy for real-time optimization of fuel economy and emissions, *SAE Paper 2000-01-1543, 2000.*

[11] N. J. Schouten, M. A. Salman, N. A. Kheir, Fuzzy logic control for parallel hybrid vehicles, *IEEE Trans. Contr. Syst. Technol., vol. 10, no. 3, pp. 460–468, May 2002.*

[12] Pérez-Pinal, F.J., Kota-Renteria, J.C., Nuñez-Perez, J.C., Al-Mutawaly, N., Hybrid conversion kit applied to public transportation: A taxi case solution, (2013) *International Review on Modelling and Simulations (IREMOS)*, 6 (2), pp. 554-559.

[13] R. Langari, W. Jong-Seob, Intelligent energy management agent for a parallel hybrid vehicle-part I: system architecture and design of the driving situation identification process, *Vehicular Technology, IEEE Transactions on, Vol. 54, Issue 3, May 2005 Page(s):925 – 934.*

[14] S. Delprat, G. Paganelli, T. M. Guerra, J. J. Santin, M. Delhom, E. Combes, Algorithmic optimization tool for the evaluation of HEV control strategies, *in Proc. Electric Vehicle Symp. 16, Beijing, China, 1999.*

[15] S. Rimaux, M. Delhom, E. Combes, Hybrid vehicle powertrain: modeling and control, *in Proc. Elect. Veh. Symp. 16, Beijing, China, Oct. 1999.*

[16] A. Brahma, Y. Guezennec, G. Rizzoni, Optimal energy management in series hybrid vehicles, *in Proc. Amer. Control Conf., Chicago, IL, June 2000.*

[17] E. D. Tate, S. P. Boyd, Finding ultimate limits of performance for hybrid electric vehicles, *SAE Paper-01-3099, 2000.*

[18] C.-C. Lin, H. Peng, J.W. Grizzle, J.-M. Kang, Power management strategy for a parallel hybrid electric truck, *IEEE Trans. Contr. Syst. Technol., vol. 11, no. 6, pp. 839–849, Nov. 2003.*

[19] S. Delprat, J. Lauber, T. M. Guerra, J. Rimaux, Control of a Parallel Hybrid Powertrain: Optimal Control, *Vehicular Technology, IEEE Transactions on, Vol. 53, Issue 3, May 2004 Page(s):872 – 881.*

[20] M. Koot, J.T.B.A. Kessels, B. de Jager, W.P.M.H. Heemels, P.P.J. van den Bosch, M. Steinbuch, Energy management strategies for vehicular electric power systems, *Vehicular Technology, IEEE Transactions on, Vol. 54, Issue 3, May 2005 Page(s):771 – 782.*

[21] Cheng-Hong Yang, Member, IAENG, Yu-Huei Cheng, and Li-Yeh Chuang: "PCR-CTPP design based on Particle Swarm Optimization with Fuzzy Adaptive Strategy", Engineering Letters, vol 20 issue 2, pp196-202, year 2012.

[22] Cyril Dennis Enyi, and Mukiawa Edwin Soh, Modified Gradient-Projection Algorithm for Solving Convex Minimization Problem in Hilbert Spaces, IAENG International Journal of Applied Mathematics, 44:3, p144-150, year 2014.

[23] Grzegorz Koloch, and Bogumil Kaminski: Nested vs. Joint Optimization of Vehicle Routing Problems with Three-dimensional Loading Constraints, Engineering Letters, vol 18, issue 2, pp193-198, year 2010.

[24] Genshun Wan, Xuehua Song, and Riccardo Bettati, An Improved EZW Algorithm and Its Application in Intelligent Transportation Systems, Engineering Letters, vol. 22, issue 2, pp63-69, year 2014.

[25] Hybrid cars, TOYOTA PRIUS web site www.toyota.com/prius/index.html?s_van=GM_TN_HYBRID_PRIUS

[26] National Renewable Energy Laboratory, Advanced Vehicle Simulator http://sourceforge.net/projects/adv-vehicle-sim/files/ADVISOR/

[27] P. Setlur, J.R. Wagner, D.M. Dawson, B. Samuels, Nonlinear control of a continuously variable transmission (CVT), *Control Systems Technology, IEEE Transactions on, Volume 11, Issue 1, Jan. 2003*

*Page(s):101 – 108.*

[28] J. M. Miller, Hybrid electric vehicle propulsion system architectures of the e-CVT type, *Power Electronics, IEEE Transactions on, Vol. 21, Issue 3, May 2006 Page(s):756 – 767.*

[29] A. Del Pizzo, S. Meo, G. Brando, A. Dannier, F. Ciancetta, An Energy Management Strategy for Fuel-cell Hybrid Electric vehicles via Particle Swarm Optimization approach, (2014) *International Review on Modelling and Simulations (IREMOS)*, 7 (4), pp. 543-553.

[30] V. Isastia, S. Meo, F. Esposito, An optimization technique for the choice of advanced automotive electrical systems, *The 5th IASTED International Conference on POWER AND ENERGY SYSTEMS ~EuroPES 2005~, June 15-17, 2005, Benalmádena, Spain.*

[31] F. Esposito, V. Isastia, S. Meo, Energy management Strategy for Automotive Electric Power System, *Przeglad Elektrotechniczny (ISSN 0033-2097), vol. 2006, n. 2, pp. 26-31*, Selected paper from International Conference on Power Electronics and Intelligent Control for Energy Conservation, PELINCEC 2005.

[32] S. Boyd, L. Vandenberghe, *Convex Optimization*, Cambridge University Press 2004.

[33] Fletcher, R., *Practical Methods of Optimization*, John Wiley and Sons, 2000.

[34] Schittkowski, K., NLQPL: A FORTRAN-Subroutine Solving constrained Nonlinear Programming Problems, *Annals of Operations Research, Vol. 5, pp 485-500, 1985.*

[35] T. Coleman, M. A. Branch, A. Grace, *Optimization Toolbox User's Guide*, The MathWorks, Inc.

**S. Meo** (M '94, SM 2004) was born in Ottaviano, Italy. He received B.S. and M.S. degrees with honours from FEDERICO II University of Naples, where currently he is an associate professor.

His current research interests include the fields of power electronics and electrical drives. He is the author of about 110 scientific publications on international Journals and international conferences in the power electronics field.

He is Editor-in-chief of the *International Review of Electrical Engineering (IREE)* and of the *International Review on Modelling and Simulations (IREMOS)*. He is reviewer for Journals and International Conferences on Power electronics and control of electrical drives.

He was involved in National Research Projects financed by the Italian Minister of the Research; He has been responsible of several contracts of advice stipulated with the Researches Centre ELASIS of FIAT, on topics of power electronics for automotive applications.

.